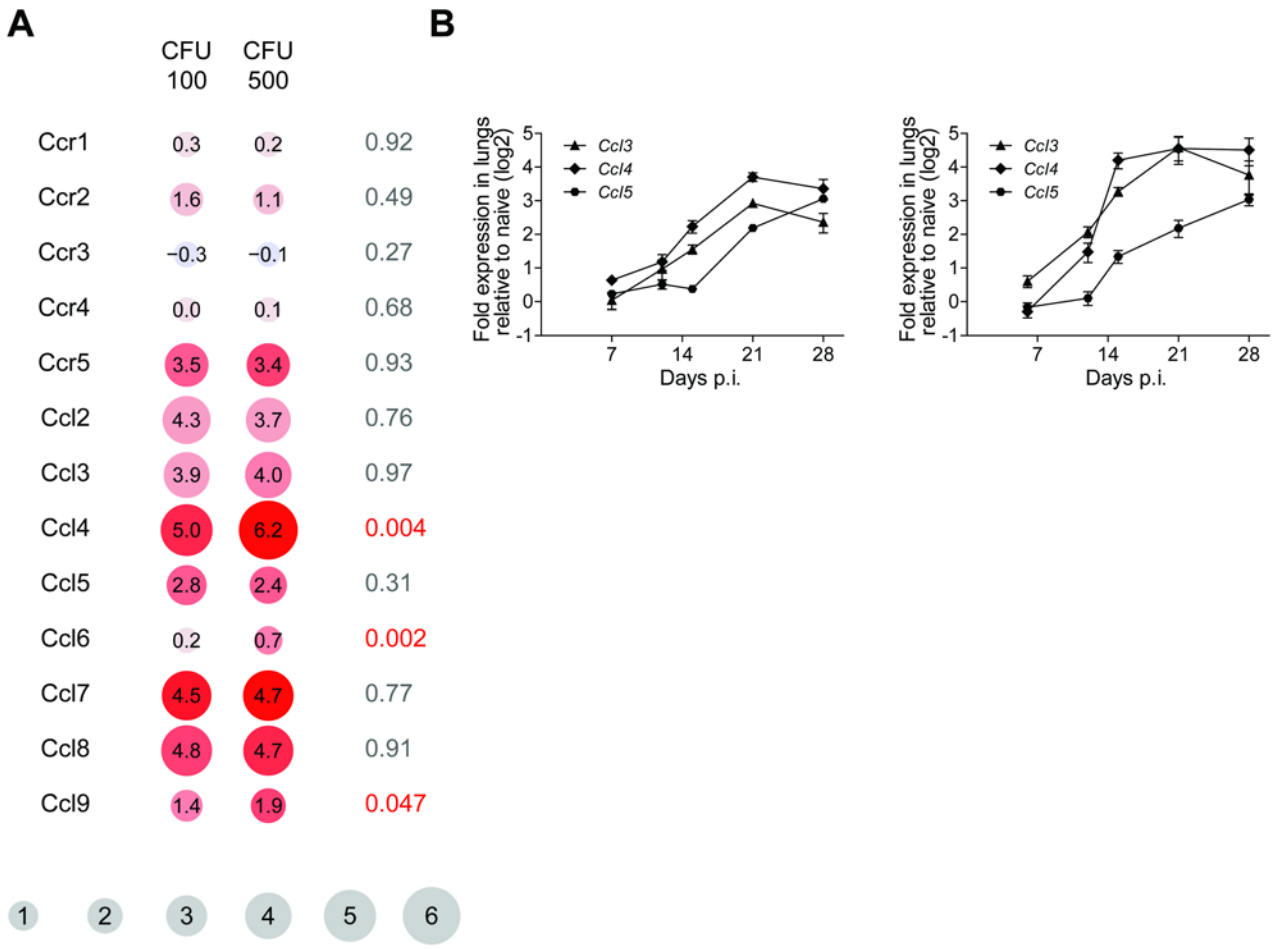

Supplemental Figure 1

Expression of CC chemokine receptors and ligands in lungs of *Mtb*-infected mice. (**A**) Effect of *Mtb* infection dose on chemokine and chemokine receptor gene expression. Comparison of microarray gene expression data between low-dose infection (100 CFUs) naïve versus day 23 p.i. with *Mtb* and high-dose infection (500 CFUs) naïve versus day 21 p.i. Lungs from five WT mice pooled for microarray analysis. Experiment performed in duplicate with color swaps. Adjusted P-value corresponds to the interaction between dosage and infection. Increasing redness stands for increased upregulation. Increasing blueness stands for increased downregulation. (**B**) Expression of chemokine mRNA at different time points p.i. in WT lungs following low-dose (left) and high-dose (right) infection relative to naïve lungs (means ± SEM; $n_{pooled} \geq 8$). Data pooled from two independent experiments.

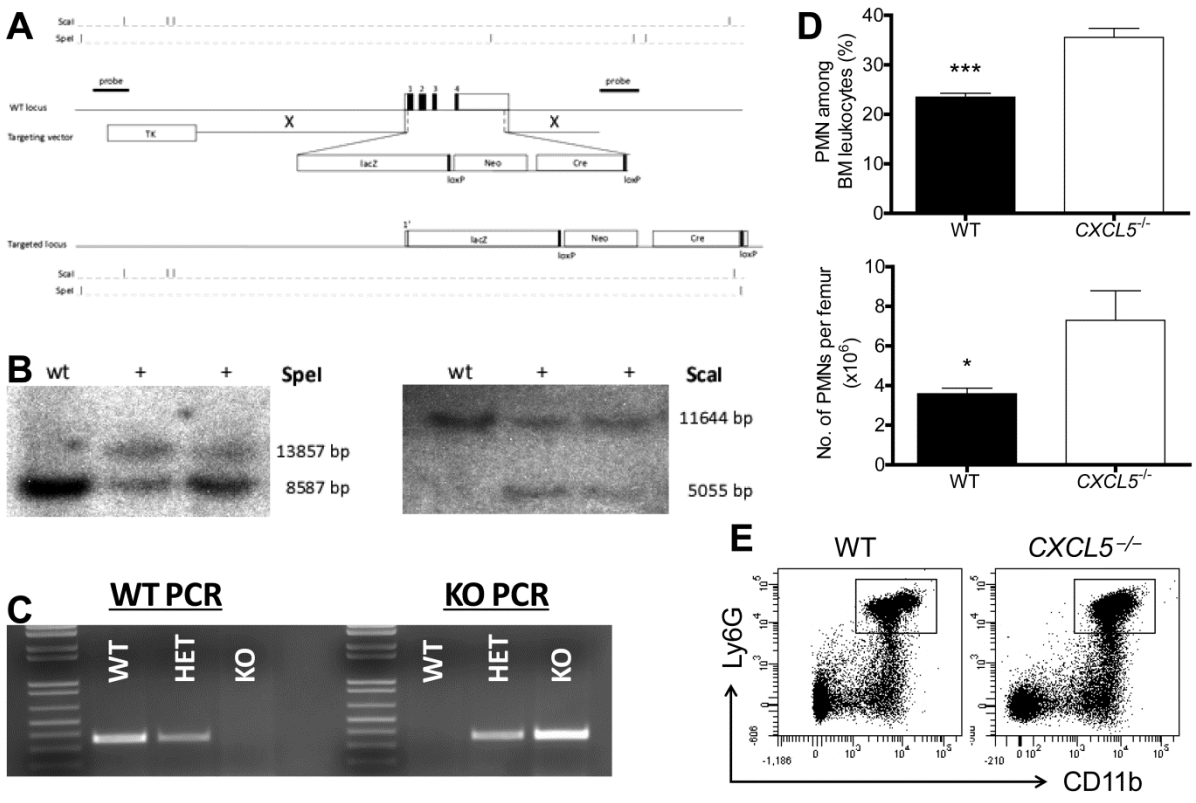

Supplemental Figure 2

Targeted disruption of *Cxcl5* gene and phenotyping of *CXCL5*$^{-/-}$ mice. (**A–B**) Targeting strategy for the murine *Cxcl5* locus, for which boxes represent exons 1 – 4; empty boxes indicate 5' and 3' non-translated regions and filled boxes represent coding regions. The locations of the probes used for ES clone verification are shown, as well as representative Southern blots below (**B**) (WT = E14 ES cells; + = targeted clones). (**C**) Mouse genotyping; left WT PCR (Primer TP1_FW: tacaagcattctcctccgattt and TP2_RV catccgcatgaatggcgagat) and right KO PCR (Primer TP1_FW: tacaagcattctcctccgattt and TP3_RV: ccttggggtcttctacctttct). In white, tail DNA from WT mice (WT), *CXCL5*$^{+/-}$ (HET) and *CXCL5*$^{-/-}$ (KO) mice. (**D**) Numbers and frequencies of PMNs among bone marrow leukocytes in naïve WT and *CXCL5*$^{-/-}$ mice determined by flow cytometry (means ± SEM; n= 5), unpaired *t*-test: * $P < 0.05$; *** $P < 0.001$. (**E**) Dot blots showing gating of PMNs (Ly6G^{hi}CD11b^{hi}) in naïve WT and *CXCL5*$^{-/-}$ mice.

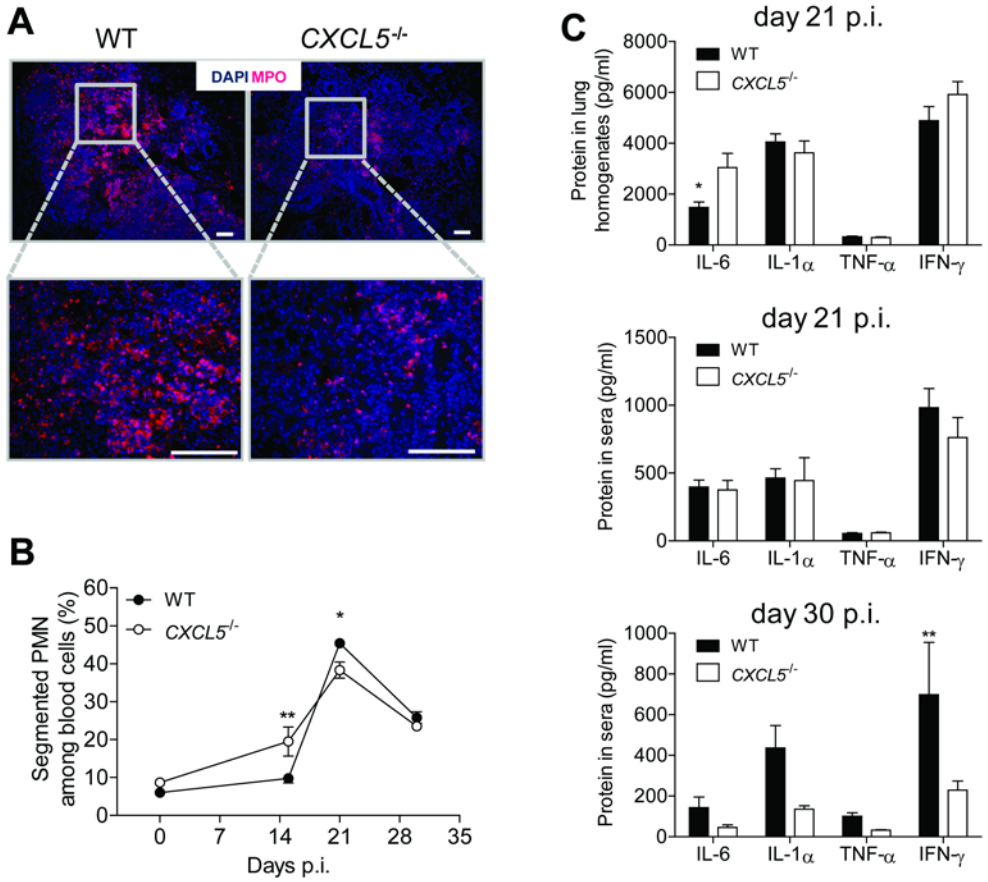

Supplemental Figure 3

Secretion of proinflammatory cytokines in *Mtb*-infected *CXCL5*$^{-/-}$ mice. (**A**) Myeloperoxidase (MPO)-positive cells in lung tissue collected at 21 days p.i., scale bars 100 µm. Representative pictures from one out of three animals are shown. (**B**) Frequencies of segmented PMNs in blood smears from WT and *CXCL5*$^{-/-}$ mice after *Mtb* infection (means ± SEM; n_{pooled} = 10). Data pooled from two independent experiments, two-way ANOVA/Bonferroni post-test. (**C**) Protein concentrations of IL-6, IL-1α, TNF-α and IFN-γ measured by multiplex analysis in lung homogenates and in sera of *Mtb*-infected WT and *CXCL5*$^{-/-}$ mice, at day 21 p.i. and day 30 p.i., respectively. Data pooled from two independent experiments (means ± SEM; n_{pooled}= 10), unpaired *t*-test. (**A, C**) Significant differences indicated by asterisks: * $P < 0.05$; ** $P < 0.01$.

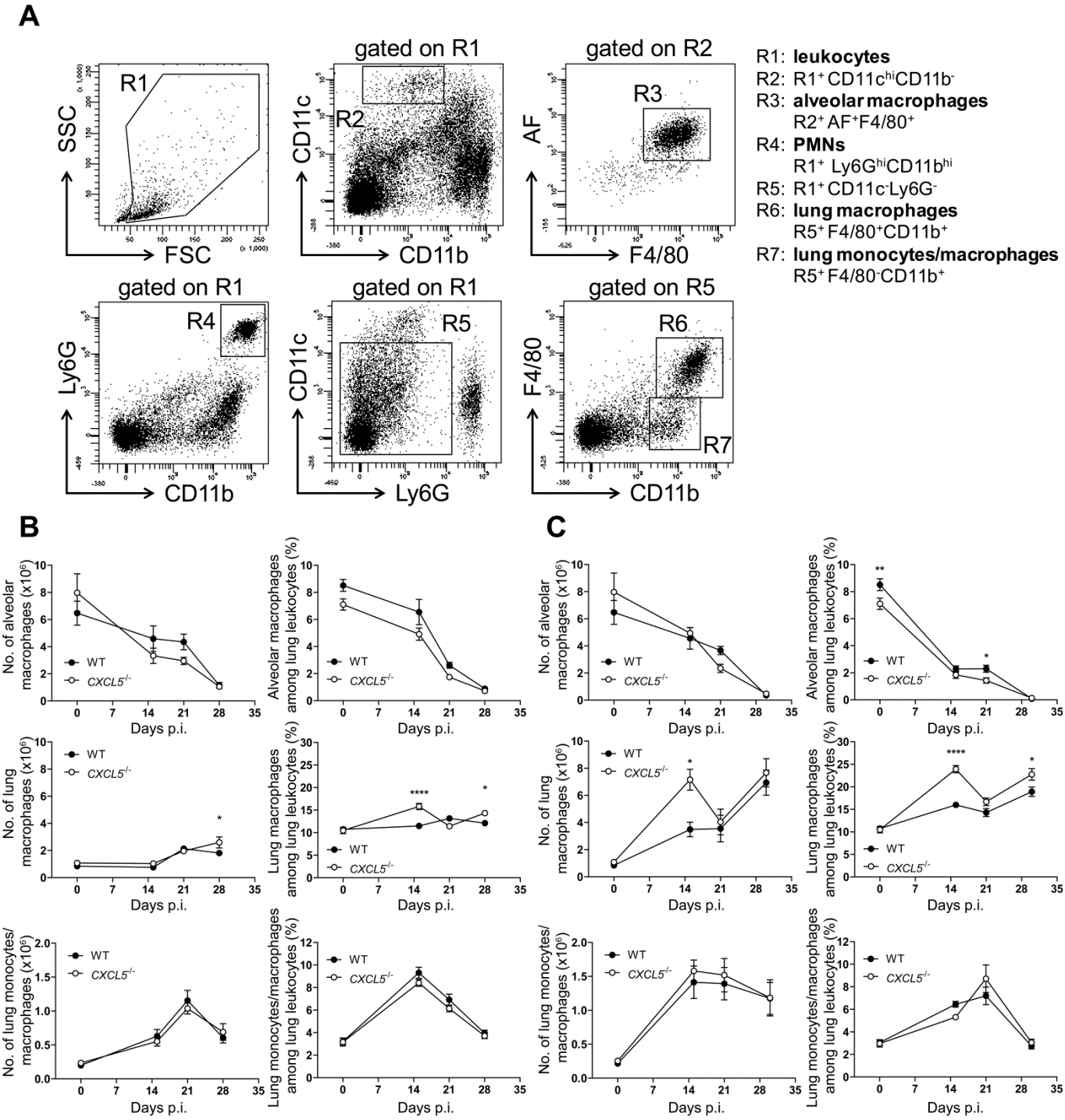

Supplemental Figure 4

Macrophages and monocytes in lungs are not affected by absence of CXCL5. (**A**) Flow cytometric gating strategy applied for identification of innate cell populations: alveolar macrophages [leukocyte gate (R1)$^+$ CD11c^{hi}CD11b$^-$ autofluorescence (AF)$^+$ F4/80$^+$], PMN [leukocyte gate (R1)$^+$ Ly6G^{hi}CD11b^{hi}], lung macrophages [leukocyte gate (R1)$^+$ CD11c$^-$Ly6G$^-$ F4/80$^+$CD11b$^+$], lung monocytes/macrophages [leukocyte gate (R1)$^+$ CD11c$^-$Ly6G$^-$ F4/80$^-$CD11b$^+$]. (**B, C**) Numbers and frequencies of alveolar macrophages, lung macrophages and lung monocytes among lung leukocytes in naïve and low- (**B**) and high-dose (**C**) *Mtb*-infected WT and *CXCL5*$^{-/-}$ mice determined by flow cytometry (means ± SEM; n_{pooled}= 10 mice per time point). Each time point shows pooled data from at least two independent experiments. Curve data pooled from a total of seven independent experiments, two-way ANOVA/Bonferroni post-test: * $P < 0.05$; ** $P < 0.01$; **** $P < 0.0001$.

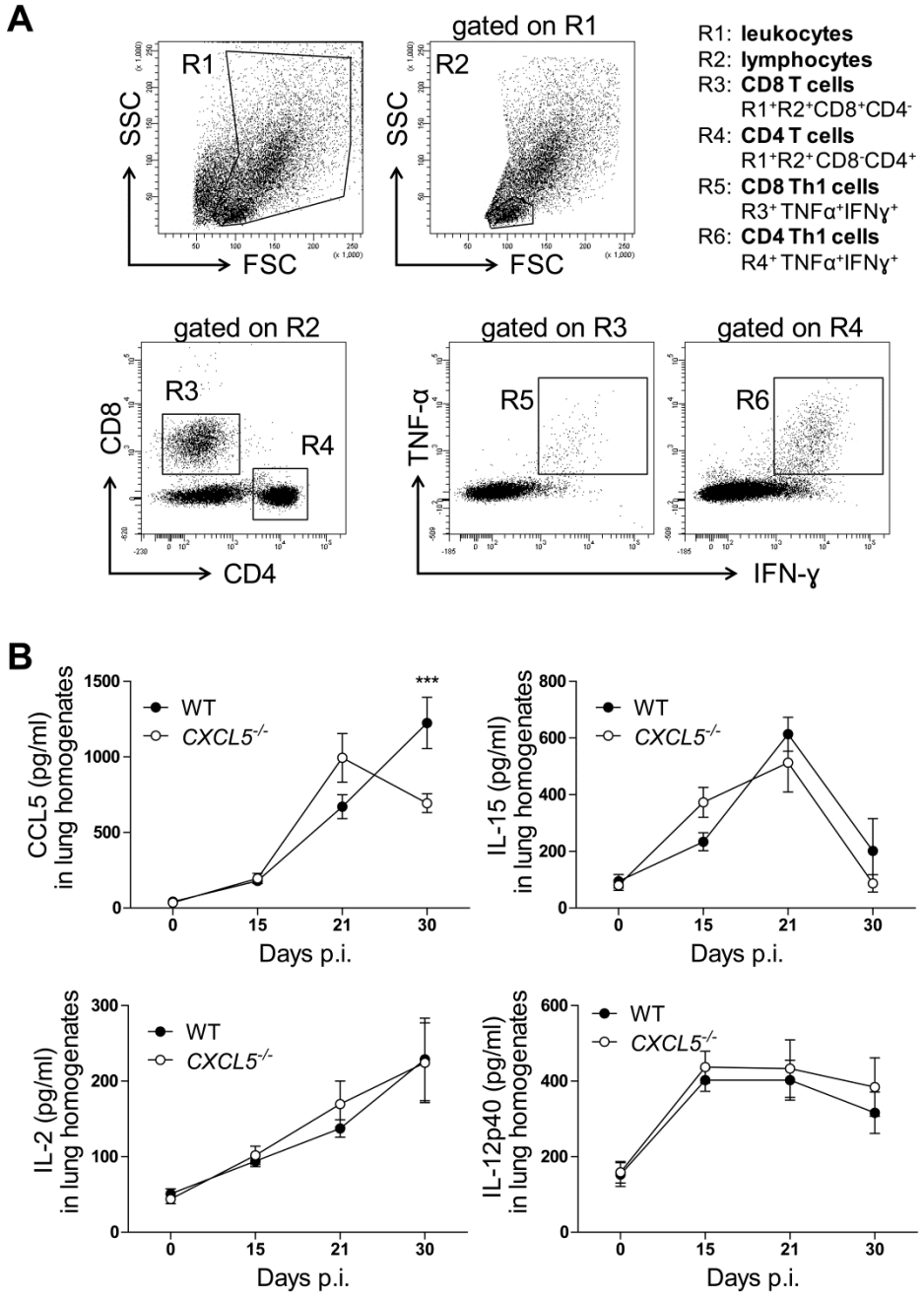

Supplemental Figure 5

T cell response-associated cytokines and chemokines are not affected by lack of CXCL5. (**A**) Flow cytometric gating strategy applied to identify *Mtb*-specific IFN-γ- and TNF-α-secreting CD4 and CD8 T cells. (**B**) Cytokine and chemokine measurements by multiplex analysis in lung homogenates of naïve and *Mtb*-infected WT and *CXCL5*$^{-/-}$ mice. Data pooled from two independent experiments (means ± SEM; n_{pooled}= 10), two-way ANOVA/Bonferroni post-test: *** $P < 0.001$.

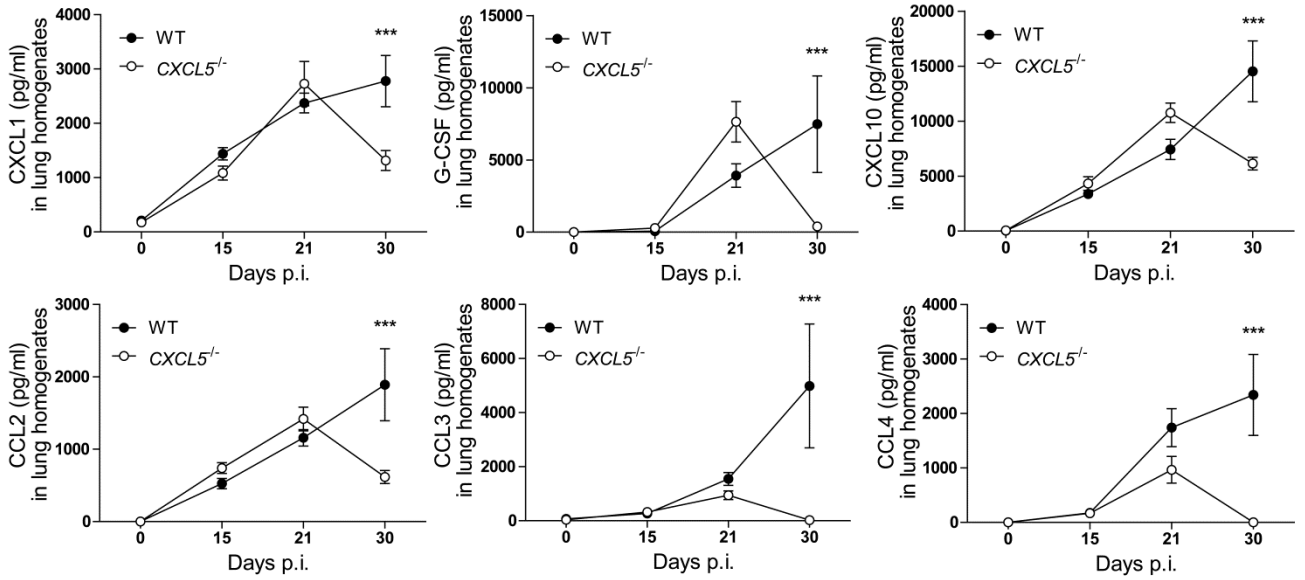

Supplemental Figure 6

Chemoattractants in lung homogenates of *Mtb*-infected mice. Chemokine measurements by multiplex analysis in lung homogenates of naïve and *Mtb*-infected WT and *CXCL5*$^{-/-}$ mice (means ± SEM; n_{pooled} = 10). Data are pooled from two independent experiments, two-way ANOVA/Bonferroni post-test: *** $P < 0.001$.

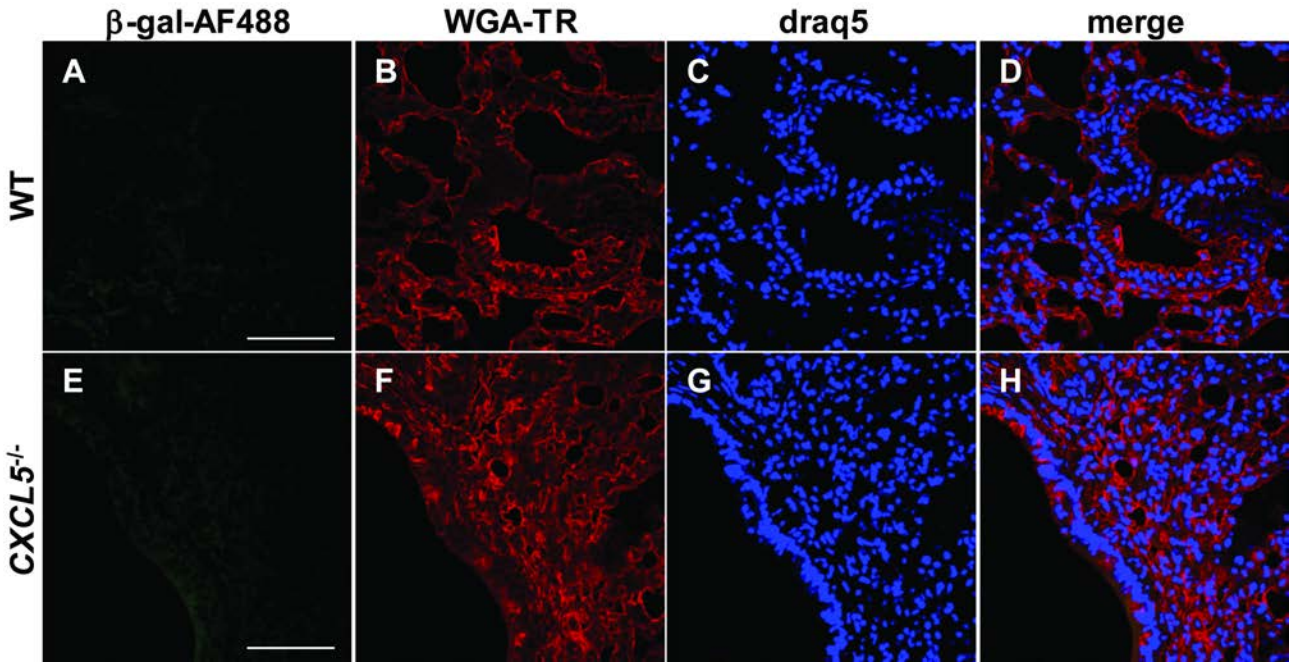

Supplemental Figure 7

Absence of *in situ* CXCL5 expression in lungs of naïve mice. Lung tissue from naïve WT control (**A–D**) and *CXCL5*$^{-/-}$ mice (**E–H**) was stained for β-galactosidase (β-gal, AF488, green) with specific antiserum. Tissue was counterstained with wheat germ agglutinin (WGA, TexasRed, red) and draq5 (blue). No nuclear β-galactosidase staining and no unspecific granular staining pattern were observed. Scale bars 50 µm (**A–H**). Representative confocal images from one experiment (n = 3).

A

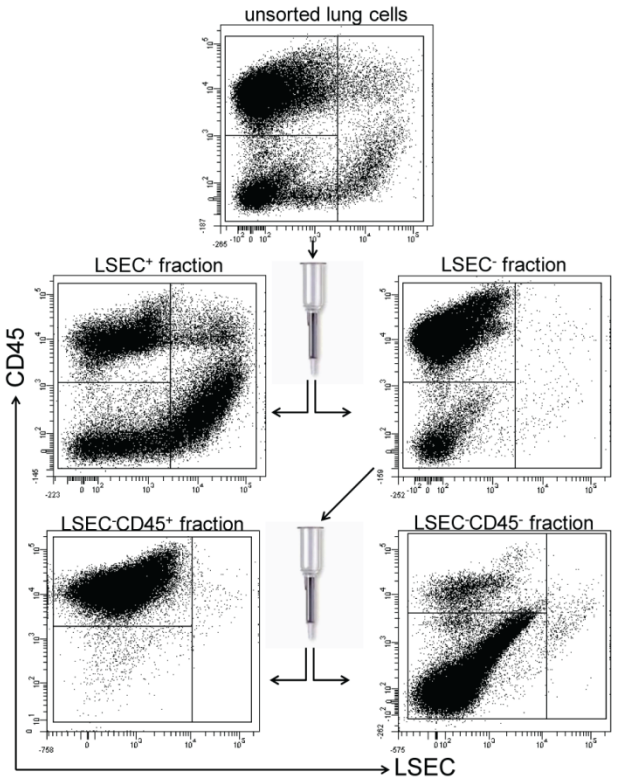

B

unsorted lung cells	
endothelial cells (LSEC$^+$)	7.2% ± 1.1%
leukocytes (LSEC$^-$CD45$^+$)	71.6% ± 1.0%
epithelial cells and rest (LSEC$^-$CD45$^-$)	21.0% ± 0.2%
LSEC$^+$ sorted fraction	
endothelial cells (LSEC$^+$)	35.2% ± 3.8%
leukocytes (LSEC$^-$CD45$^+$)	43.5% ± 3.1%
epithelial cells and rest (LSEC$^-$CD45$^-$)	20.8% ± 1.4%
LSEC$^-$CD45$^+$ sorted fraction	
endothelial cells (LSEC$^+$)	0.33% ± 0.1%
leukocytes (LSEC$^-$CD45$^+$)	98.2% ± 0.2%
epithelial cells and rest (LSEC$^-$CD45$^-$)	1.2% ± 0.1%
LSEC$^-$CD45$^-$ sorted fraction	
endothelial cells (LSEC$^+$)	1.2% ± 0.3%
leukocytes (LSEC$^-$CD45$^+$)	15.6% ± 4.2%
epithelial cells and rest (LSEC$^-$CD45$^-$)	83.0% ± 3.9%

Frequencies of gated cell population before and after MACS sort from *Mtb* infected WT lungs at day 21 p.i. (n = 3, mean ± SEM).

C

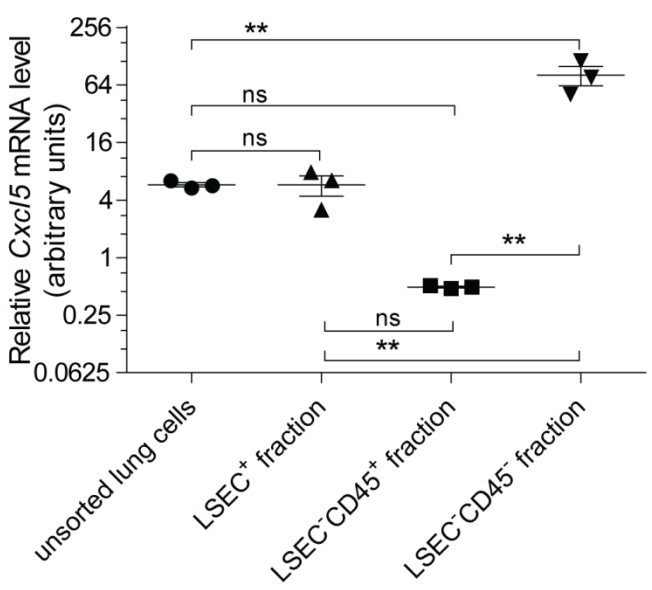

Supplemental Figure 8

Cxcl5 mRNA by MACS-sorted epithelial cell fraction. (**A**) Dot blots indicating two-step MACS sorting strategy. Cells from *Mtb* infected WT mice were sorted according to LSEC (endothelial cell marker) expression. Then, cells in the LSEC$^-$ fraction were sorted according to CD45 (leukocyte marker) expression. (**B**) Purity of sorted cell fractions (gating indicated in (A); endothelial cells (LSEC$^+$), leukocytes (LSEC$^-$CD45$^+$) and epithelial cells plus rest (LSEC$^-$ CD45$^-$) were analyzed by flow cytometry. (**C**) Relative *Cxcl5* mRNA abundance in sorted cell populations from high-dose *Mtb*-infected WT mice measured by quantitative RT-PCR of *Cxcl5* and *Gapdh* mRNA expression; [formula: $1.8^{(ct\ Gapdh\ -\ ct\ Cxcl5)}$ x 100]; (means ± SEM, n = 3), one-way ANOVA/Bonferroni post-test. Data from one experiment. Significant differences indicated by asterisks: ** $P < 0.01$; ns, $P > 0.05$.